Apalowo, R.K. and Chronopoulos, D. and Ichchou, M. and Essa, Y. and Martin De La Escalera, F. (2017) The impact of temperature on wave interaction with damage in composite structures. Proceedings of the Institution of Mechanical Engineers, Part C: Journal of Mechanical Engineering Science, 231 (16). pp. 3042-3056. ISSN 0954-4062

The impact of temperature on wave interaction with damage in composite structures

R.K. Apalowo[a], D. Chronopoulos[a], M. Ichchou[b], Y. Essa[c], F. Martin De La Escalera[c]

[a]*Institute for Aerospace Technology & The Composites Research Group, The University of Nottingham, NG7 2RD, UK*
[b]*Ecole Centrale de Lyon, 36 Avenue Guy de Collongue, 69130 Ecully, France*
[c]*Aernnova Engineering Solutions Iberica, Madrid, Spain*

Abstract

The increased use of composite materials in modern aerospace and automotive structures, and the broad range of launch vehicles' operating temperature imply a great temperature range for which the structures has to be frequently and thoroughly inspected. A Thermal Mechanical Analysis (TMA) is used to experimentally measure the temperature dependent mechanical properties of a composite layered panel in the range of -100°C to 150°C. A hybrid wave finite element (WFE)/finite element (FE) computational scheme is developed to calculate the temperature dependent wave propagation and interaction properties of a system of two structural waveguides connected through a coupling joint. Calculations are made using the measured thermomechanical properties. Temperature dependent wave propagation constants of each structural waveguide are obtained by the WFE approach and then coupled to the fully FE described coupling joint, on which damage is modelled, in order to calculate the scattering magnitudes of the waves interaction with damage across the coupling joint. The significance of the panel's glass transition range on the measured and calculated properties is emphasised. Numerical results are presented as illustration of the work.

Keywords: Temperature dependent mechanical characteristics, Wave propagation properties, Damage detection, Wave finite element, Composite structure

Email addresses: eaxrka@nottingham.ac.uk (R.K. Apalowo), Dimitrios.Chronopoulos@nottingham.ac.uk (D. Chronopoulos)

Contents

1. Introduction

Composite structures are being increasingly used in many industrial fields, such as aerospace and military, due to their versatile physical and mechanical properties. However, aerospace and automotive structures operate within varying temperature range, which is typically from -100°C to +200°C for launch vehicles and from -60°C to +50°C for aircraft and automobile structures. Despite their versatility, composite structures may exhibit a great variety of structural failure modes for which they must be thoroughly inspected in order to ensure continuous usage and structural integrity. These modes which include delamination, notch, fibre breakage, matrix crack and debonding, occur mainly as a result of loads during service and inaccuracies during manufacturing. Aeronautics industries spend approximately 27% of an average modern aircraft's lifecycle cost on offline inspection and repair of the structural failures [1]. Therefore, the non-destructive damage detection and evaluation is of paramount importance for monitoring the condition and residual life estimation of in-service aerospace structures. Of particular interest is thermal dependent damage detection in composite layered structures.

Thermomechanical behaviour of laminated structures have been conducted on various topics. In [2], the elastodynamic response of a polymeric laminate subjected to a discrete range of temperatures at a constant relative humidity is studied, with damping and dynamic longitudinal elastic modulus presented as a function of temperature dependent. In [3, 4], the temperature dependent elastic constant and dynamic shear properties of an epoxy resin and its carbon fibre-reinforced composite are presented. More recently, the effect of high temperature on the thermomechanical response of various composite structures, such as multi-layered plates and shells [5], glass epoxy composites [6, 7] and carbon fibre epoxy composites [8], [9], has been extensively assessed. Moreover, temperature dependent wave based detection of structural damage has been an extensive field of study over the recent years. In [10, 11] baseline subtraction approach is used to predict temperature effect on guided wave signal and to optimally enhance the long term stability of the signal. The approach is extended in [12, 13] to reduce the number of baseline measurements to be used. Pitch-catch approach is used to numerically predict and experimentally measure the effect of low [14] as well as moderately [15] and extremely [16] elevated temperature on the lamb wave response in sandwich panels and aluminium plates respectively. This is extended in [17] to cover a wider range of temperature in a large frequency range. Semi analytical finite element (SAFE) model is developed in [18] to predict guided wave response under varying temperature in plate. More recently co-integration technique is developed to control the effect of varying temperature in damage detection of structure based on spectral lines analysis [19, 20], wavelet decomposition [21] and direct Lamb wave responses [22]. To the best of the authors' knowledge, FE based computational scheme is quite limited in this field of research and the investigation of thermal effect on wave interaction in complex and arbitrarily layered composite structures is almost in-existent in the open literature.

Wave based damage detection methods are based on calculating the reflection and transmission coefficients at the point of inhomogeneity or structural discontinuity. The inhomogeneity can be in the form of joints such as point and finite joint [23], beam connection [24], plate and stiffened rib connection [25], angled joint [26], curved junction [27], T-junction [28] and L-junction [29, 30], or in form of defects, such as crack [31] and delamination [32] along the structure. It has been shown that a fraction of an incident wave will be reflected due to an interaction with any of these

forms of inhomogeneity. Calculations of the scattering coefficients and vibrational response have been exhibited using various numerical methods, such as spectral element method [33], boundary element method [34], finite element method [35], decomposition method [36] and probabilistic optimisation [37]. Other methods include combined Wave and Finite Element (WFE) method [30, 38], finite and spectral element method [39] and finite and strip element method [40]. Among these numerical methods, the WFE method [30, 38, 41, 42] is one of the most efficient computational methods suitable for predicting the vibrational response and wave interaction with damage in various types of structures. The method has recently found applications in predicting the vibroacoustic and dynamic performance of composite panels and shells [43–45], with pressurized [46] and complex periodic structures [47–49] having been investigated. The variability of acoustic transmission through layered structures [50], as well as wave steering effects in anisotropic composites [51] have been modelled through the same methodology. Therefore, application of this method to predict thermal effect on wave interaction in composite structure will be a significant contribution to the field of non-destructive damage detection using wave based models.

The main novelty of this article is to exhibit the effect of temperature on the wave properties of a composite layered panel and consider the interaction of the waves with damage as a function of temperature. The temperature dependent mechanical properties of a carbon epoxy facesheet material and a honeycomb core material, constituting the layered panel, are experimentally calculated using a Thermal Mechanical Analysis. A structural system consisting of two healthy waveguides connected by a coupling joint, on which damage is described, is considered. A wave finite element approach is used to calculate the wave propagation constants of each waveguide. These are then coupled to standard finite element model of the coupling joint, in order to calculate waves-damage interaction scattering coefficients. All calculations are temperature dependent.

The paper is organised as follows. Section 2 presents the experimental measurement of the temperature dependent mechanical properties of the facesheet and core materials. Section 3 presents the calculations of temperature dependent wave properties and dispersion characteristics, as well as the computation of temperature dependent wave scattering properties. Numerical results are presented in Section 4 together with a discussion of the findings. Finally, Section 5 presents concluding remarks of the work.

2. Measurement of Temperature Dependent Mechanical characteristics

A Thermal Mechanical Analysis (TMA) device is used to measure the temperature dependent sandwich panel comprising of a carbon epoxy facesheet and a quasi-isotropic honeycomb core, which absorbs and adheres to the resin in which the facesheet is impregnated. In the polymerisation process, the resin serves as the facesheet matrix as well as the binding agent. The nominal mechanical characteristics of the composite panel's constituents at $20°C$ are shown in Table 1.

[Table 1 about here.]

[Figure 1 about here.]

Measurements are made at a temperature range of -5°C to 150°C and then extrapolated for the results of temperatures up to -100°C by assuming smooth quadratic expansion of the curves. This extrapolation is done to capture the lower limits of the operating temperature range of the composite panel as an aerospace structure. Such extrapolation is generally acceptable for composite materials having no significant transition (such as crystallisation) in their metallography structure at low temperature range (such as those below -5°C). Temperature dependent Young's modulus of the facesheet material is measured using the TMA device, as shown by configuration in Fig. 1, by subjecting a segment of the facesheet to an initial longitudinal traction test before imposing a 1 Hz excitation as displacement to the segment. The corresponding material loss factor is determined as $tan\delta = \mathrm{E}^1/\mathrm{E}^2$, where δ is the phase lag between the stress and strain, E^1 the loss modulus and E^2 the storage modulus of the material. A reduction ratio, R_f, calculated as $\mathrm{R}_f = \mathrm{E}_a/\mathrm{E}_n$ is determined at each temperature of the measured Young's modulus, with E_a the measured (actual) values at respective temperature and E_n the nominal value as given in Table 1. This is used to calculate the actual values of other mechanical characteristics of the material as $\mathrm{E}_a = \mathrm{R}_f \times \mathrm{E}_n$ at each corresponding temperature using the nominal value of each of the mechanical characteristics. The results of the experimental measurements and the corresponding material loss factor are presented in Fig. 2. Measured elastic modulus decreases while the corresponding material loss factor increases slightly with temperature until $110°C$, where the glass transition of the resin occurs. There

is a drastic increase of the loss factor to the peak level at this temperature range. Beyond this temperature, the elastic modulus decreases rapidly with temperature while the loss factor decreases, then start increasing again due to the high viscosity of the resin at this temperature.

[Figure 2 about here.]

[Figure 3 about here.]

[Figure 4 about here.]

On the other hand, temperature dependent shear modulus of the honeycomb core is measured using the TMA machine by subjecting a segment of the core to shear deformation as shown in the configuration in Fig. 3. In order to avoid any influence of the elasticity of the facesheet on the shear deformation of the core's segment, a steel sheet layer is attached on it to increase its rigidity. Similar calculations, as described in the Young's modulus measurement, are carried out to determine the shear modulus and the corresponding dissipation ratios of the quasi-isotropic honeycomb core. The results of the temperature dependent shear modulus measurements and corresponding dissipation ratios are shown in Fig. 4. Results measured in this case show similar trend as in the case of the facesheet material.

3. Calculation of Temperature Dependent Wave characteristics

3.1. Wave Propagation Modelling

One dimensional elastic wave propagation along x direction of an arbitrarily layered sandwich panel is considered. A segment of the periodic waveguide is meshed using a single finite element along the axis of wave propagation and an arbitrary number of elements in other directions Fig. 6. The left and right hand sides of the segment both have the same number of nodes and degrees of freedom (DOFs) [52]. The problem can be condensed using the transfer matrix approach [53]. The temperature and frequency dependent dynamic stiffness matrix (DSM) is determined as

$$\mathbf{D}(\omega, T) = \mathbf{K}(T) - \omega^2\mathbf{M}(T) + i\omega\mathbf{C}(T) \tag{1}$$

where **K**, **M** and **C** are the stiffness, mass and damping matrices of the FE model for each considered temperature T.

The dynamic equilibrium of the model is obtained by partitioning the DSM with respect to the the left, right and internal DoFs of the segment as

$$\begin{bmatrix} \mathbf{D}_{LL} & \mathbf{D}_{LI} & \mathbf{D}_{LR} \\ \mathbf{D}_{IL} & \mathbf{D}_{II} & \mathbf{D}_{IR} \\ \mathbf{D}_{RL} & \mathbf{D}_{RI} & \mathbf{D}_{RR} \end{bmatrix} \begin{Bmatrix} \mathbf{q}_L \\ \mathbf{q}_I \\ \mathbf{q}_R \end{Bmatrix} = \begin{Bmatrix} \mathbf{F}_L \\ \mathbf{F}_I \\ \mathbf{F}_R \end{Bmatrix} \tag{2}$$

[Figure 5 about here.]

where **q** and **F** are the displacement and internal force vectors respectively. The internal force vector responsible for transmitting the wave from one element to the other within the structure, hence it is non-zero, even for a free wave motion where no external load is applied [52]. In the case where no external forces are exerted on the internal nodes ($\mathbf{F}_I = 0$), classical condensation techniques [54], such as the Guyan-type condensation, is applied to condense the internal DoFs entries as given in Eq. (2). The finite element mesh of the section of the segment with the internal nodes condensed is shown in Fig. 5.

$$\begin{bmatrix} \mathbf{D}_{LL} - \mathbf{D}_{LI}\mathbf{D}_{II}^{-1}\mathbf{D}_{IL} & \mathbf{D}_{LR} - \mathbf{D}_{LI}\mathbf{D}_{II}^{-1}\mathbf{D}_{IR} \\ \mathbf{D}_{RL} - \mathbf{D}_{RI}\mathbf{D}_{II}^{-1}\mathbf{D}_{IL} & \mathbf{D}_{RR} - \mathbf{D}_{RI}\mathbf{D}_{II}^{-1}\mathbf{D}_{IR} \end{bmatrix} \begin{Bmatrix} \mathbf{q}_L \\ \mathbf{q}_R \end{Bmatrix} = \begin{Bmatrix} \mathbf{F}_L \\ \mathbf{F}_R \end{Bmatrix} \tag{3}$$

$$\begin{bmatrix} \mathbf{D}^*_{LL} & \mathbf{D}^*_{LR} \\ \mathbf{D}^*_{RL} & \mathbf{D}^*_{RR} \end{bmatrix} \begin{Bmatrix} \mathbf{q}_L \\ \mathbf{q}_R \end{Bmatrix} = \begin{Bmatrix} \mathbf{F}_L \\ \mathbf{F}_R \end{Bmatrix} \tag{4}$$

where the matrix $\mathbf{D}^*$ is the reduced dynamic stiffness matrix. Therefore, the continuity condition and equilibrium of forces equations at the interface of two consecutive periodic segments r and $r+1$ are given as

$$\mathbf{q_R}^{(r)} = \mathbf{q_L}^{(r+1)}; \mathbf{F_R}^{(r)} = -\mathbf{F_L}^{(r+1)} \tag{5}$$

Combining Eqs. 4 and 5, gives the relation of the displacement and force vectors of the left hand side and the right hand side of the segment as

$$\begin{Bmatrix} \mathbf{q_R}^{(r)} \\ \mathbf{F_R}^{(r)} \end{Bmatrix} = \begin{Bmatrix} \mathbf{q_L}^{(r+1)} \\ -\mathbf{F_L}^{(r+1)} \end{Bmatrix} = \mathbf{T} \begin{Bmatrix} \mathbf{q_L}^{(r)} \\ \mathbf{F_L}^{(r)} \end{Bmatrix} \tag{6}$$

where matrix $\mathbf{T}$ is the transfer matrix expressed as

$$\mathbf{T} = \begin{bmatrix} -\mathbf{D}^*_{LR}{}^{-1}\mathbf{D}^*_{LL} & \mathbf{D}^*_{LR}{}^{-1} \\ -\mathbf{D}^*_{RL} + \mathbf{D}^*_{RR}\mathbf{D}^*_{LR}{}^{-1}\mathbf{D}^*_{LL} & -\mathbf{D}^*_{RR}\mathbf{D}^*_{LR}{}^{-1} \end{bmatrix} \tag{7}$$

As the wave is propagating only in the x-direction, a constant of propagation, λ, relates the left side's displacement and internal force of the segment to that of the right side according to the Bloch's theorem [55] as

$$\lambda \mathbf{q}_L{}^{(r)} = \mathbf{q}_R{}^{(r)}; -\lambda \mathbf{F}_L{}^{(r)} = \mathbf{F}_R{}^{(r)} \tag{8}$$

Combining Eqs.6 and 8, the free wave propagation can be defined by the eigenvalue problem

$$\mathbf{T} \begin{Bmatrix} \mathbf{q_L}^{(r)} \\ \mathbf{F_L}^{(r)} \end{Bmatrix} = \lambda_j \begin{Bmatrix} \mathbf{q_L}^{(r)} \\ \mathbf{F_L}^{(r)} \end{Bmatrix} \tag{9}$$

whose solution yields the temperature dependent constant of propagation, λ_j and the wavenumbers, k_j as

$$k_j(\omega, T) = -\frac{\ln\left(\lambda_j(\omega, T)\right)}{i\delta_x}, j = 1, 2, ..., 2n \tag{10}$$

where subscript j corresponds to wave type j and n the number of DoFs one side of the segment and δ_x the length of a periodic segment.

The wave modes obtained at each frequency and temperature is post processed and partitioned as

$$\mathbf{\Phi} = \begin{bmatrix} \mathbf{\Phi}_q{}^{inc} & \mathbf{\Phi}_q{}^{ref} \\ \mathbf{\Phi}_F{}^{inc} & \mathbf{\Phi}_F{}^{ref} \end{bmatrix} \tag{11}$$

where inc and ref denote the positive and negative going waves respectively. Assuming modal decomposition,

$$\left\{ \begin{array}{c} \mathbf{q_L} \\ \mathbf{F_L} \end{array} \right\}^{(k)} = \mathbf{\Phi} \left\{ \begin{array}{c} \mathbf{Q}^{inc} \\ \mathbf{Q}^{ref} \end{array} \right\}^{(k)} \tag{12}$$

where $\mathbf{Q}$ denotes the amplitudes of the wave modes. The physical domain, where the motion is represented in terms of displacements and nodal forces, has been transformed into the wave domain, where the motion is described in terms of the incident and reflected wave amplitudes.

3.2. Wave Dissipation Modelling

The governing displacement relation for time harmonic wave motion, according to Bloch's theorem [55] can be given as

$$w = We^{i(\omega t - kx)} \tag{13}$$

where w is the displacement of the wave motion, W the maximum amplitude, k the wavenumber, x the axial distance travelled along the structure, t the time and ω the wave frequency.

The dissipation ratio of the wave after travelling over a certain length along the structure can be determined as

$$d_r = 10 \log \frac{A_1}{A_0} \tag{14}$$

d_r is the dissipation loss of the travelling wave in decibel per unit length, A_0 and A_1 the amplitudes at the reference points in consideration. The amplitudes of the wave, A_0 and A_1, at a reference points x_0 and x_1, can be expressed as

$$A_0 = Ae^{i(\omega t - kx_0)}; A_1 = Ae^{i(\omega t - kx_1)} \tag{15}$$

where A is the maximum amplitude of the wave. Eq. (14) can be transformed into

$$d_r = 10 \frac{\ln \frac{A_1}{A_0}}{\ln 10} \tag{16}$$

which can be combined with Eq. (15) and considering the that ω and t are constant at the two reference points. Upon evaluating the expression obtained, the wave dissipation loss per unit

length can then be given as

$$d_r = 10\frac{|k_{im}|}{\ln 10} \tag{17}$$

where $|k_{im}|$ is the absolute value of the imaginary part of the wavenumber.

3.3. Calculation of Wave Scattering Coefficients

The degree of wave scattering, due to wave interaction with damage along the system, is determined using the modes properties of the waves that impinges on the damage. The reflection coefficient is the fraction of the incident wave reflected while the transmission coefficient is the fraction of the wave transmitted beyond the damage. As the wave propagation is unidirectional and impinging at 90^o, no refraction is expected.

[Figure 6 about here.]

The description of the system is based on the assembly of a number of identical waveguides connected through a joint, referred to as the coupling element/joint. A system of two coplanar waveguides connected through a coupling joint, as shown in Fig. 6, is considered. In this approach, the connecting surfaces of the waveguides with the coupling element must have the same mesh. The method can be extended to n number of waveguides [56] and to waveguides connected at angles [30]. Waves propagate from the two healthy waveguides through the joint on which structural damage (notch or crack) is modelled. Wave interaction coefficients are calculated by coupling the WFE calculated wave propagation constants of the waveguides to the standard FE model of the joint.

The coupling joint is modelled in a similar manner as described in Section 3.1, but its segment is fully meshed (using its whole length) along the axis of wave propagation rather than using a single element as in the case of the WFE model. Its DSM are partitioned, into corresponding components of interface and non-interface nodes in the waveguides-coupling joint assembly, as

$$\begin{bmatrix} \mathbf{D}_{11} & \mathbf{D}_{12} \\ \mathbf{D}_{21} & \mathbf{D}_{22} \end{bmatrix} \begin{Bmatrix} \mathbf{q}_1 \\ \mathbf{q}_2 \end{Bmatrix} = \begin{Bmatrix} \mathbf{F}_1 \\ \mathbf{F}_2 \end{Bmatrix} \tag{18}$$

where subscript 1 corresponds to the DoFs of the interface nodes of the two waveguides with the coupling joint, and subscript 2, the non-interface nodes. Eq. (18) can then be condensed to determine the dynamic stiffness matrix, $\mathbf{D_C}^*$, of the interface nodes' DoFs in the assembly, as given in Eq. (15).

$$\mathbf{D}_\mathbf{C}^* = \mathbf{D_{11}} - \mathbf{D_{12}}\mathbf{D}_\mathbf{22}^{-1}\mathbf{D_{21}} \tag{19}$$

With the assumption of a similar mesh at the connecting interface, then the nodal displacement and internal force vectors can be given as

$$\left\{ \begin{array}{c} \mathbf{q}_{C,L} \\ \mathbf{q}_{C,R} \end{array} \right\} = \left\{ \begin{array}{c} \mathbf{q}_{1R} \\ \mathbf{q}_{2L} \end{array} \right\}; \left\{ \begin{array}{c} \mathbf{F}_{C,L} \\ \mathbf{F}_{C,R} \end{array} \right\} = \left\{ \begin{array}{c} \mathbf{F}_{1R} \\ \mathbf{F}_{2L} \end{array} \right\} \tag{20}$$

where subscripts 1 and 2 denote the waveguides to the left and right sides of the coupling joint respectively. The dynamic equilibrium equation of the assembly can then be given as

$$\mathbf{D}_C{}^* \left\{ \begin{array}{c} \mathbf{q}_{1R} \\ \mathbf{q}_{2L} \end{array} \right\} = \left\{ \begin{array}{c} \mathbf{F}_{1R} \\ \mathbf{F}_{2L} \end{array} \right\} \tag{21}$$

Eq. (21) in wave domain is given as

$$\mathbf{D}_C{}^* \left[\begin{array}{c} \mathbf{\Phi}_{q1}{}^{inc}\mathbf{Q}_1{}^{inc} + \mathbf{\Phi}_{q1}{}^{ref}\mathbf{Q}_1{}^{ref} \\ \mathbf{\Phi}_{q2}{}^{inc}\mathbf{Q}_2{}^{inc} + \mathbf{\Phi}_{q2}{}^{ref}\mathbf{Q}_2{}^{ref} \end{array} \right] = \left[\begin{array}{c} \mathbf{\Phi}_{F1}{}^{inc}\mathbf{Q}_1{}^{inc} + \mathbf{\Phi}_{F1}{}^{ref}\mathbf{Q}_1{}^{ref} \\ \mathbf{\Phi}_{F2}{}^{inc}\mathbf{Q}_2{}^{inc} + \mathbf{\Phi}_{F2}{}^{ref}\mathbf{Q}_2{}^{ref} \end{array} \right] \tag{22}$$

22 can be rearranged in terms of the amplitudes of reflected and incident waves, and simplified as

$$\left\{ \begin{array}{c} \mathbf{Q}_1{}^{ref} \\ \mathbf{Q}_2{}^{ref} \end{array} \right\} = \mathbf{S} \left\{ \begin{array}{c} \mathbf{Q}_1{}^{inc} \\ \mathbf{Q}_2{}^{inc} \end{array} \right\} \tag{23}$$

where

$$\mathbf{S} = -\left[\left(\begin{array}{cc} \mathbf{\Phi}_{F1}{}^{ref} & 0 \\ 0 & \mathbf{\Phi}_{F2}{}^{ref} \end{array} \right) - \mathbf{D}_C{}^* \left(\begin{array}{cc} \mathbf{\Phi}_{q1}{}^{ref} & 0 \\ 0 & \mathbf{\Phi}_{q2}{}^{ref} \end{array} \right) \right]^{-1} \left[\left(\begin{array}{cc} \mathbf{\Phi}_{F1}{}^{inc} & 0 \\ 0 & \mathbf{\Phi}_{F2}{}^{inc} \end{array} \right) - \mathbf{D}_C{}^* \left(\begin{array}{cc} \mathbf{\Phi}_{q1}{}^{inc} & 0 \\ 0 & \mathbf{\Phi}_{q2}{}^{inc} \end{array} \right) \right] \tag{24}$$

4. Numerical Results

The application of the approach developed is applied to the layered panel for predicting its temperature dependent wave propagation constants and wave interaction scattering coefficients as presented in Section 3. Calculations are made over temperature range of -100°C to 150°C. FE modelling is done in ANSYS 14.0. The layered panel is meshed using SOLID185 elements, which comprises a 3D displacement fields and is defined by eight nodes having three degrees of freedom at each node: translations in the nodal x, y, and z directions. It also possesses formulation capability for simulating viscoelastic layered structures [57]. The temperature dependent mass and stiffness matrices extracted from the FE solution of the modelling analysis in ANSYS are post-processed in MATLAB to obtain the required wave properties of the model as discussed Section 3.

4.1. Temperature Dependent Wave Properties

The temperature dependent wave propagation constants of the viscoelastic layered panel is sought as presented in Sections 3.1 and 3.2. The panel's temperature dependent mechanical properties (elastic and shear moduli) and their respective material loss factor of the materials are presented in Figs. 2 and 4. The thickness of the core, h_c, is 12.7 mm while that of the facesheet, h_c, is 1.0 mm. The dimension of the panel is 1.0 mm $\times$ 1.0 mm. The finite element model of the panel is made using eight elements to discretise each of the facesheets and five elements to discretise the core, resulting in a total of twenty-one elements.

[Figure 7 about here.]

[Figure 8 about here.]

The wavenumber plots of the propagating waves along the panel are shown in Figs. 7 and 8. Four propagating waves, in-plane and out-of-plane flexural waves as well as torsional and axial waves, exist below the frequency of 10 kHz. The cut-on frequencies and number of waves within the considered frequency range depend on temperature as shown in Fig. 7. While at $25°C$, there are nine waves within the the frequency range with cut-ons occurring at about 10kHz, 18kHz, 25kHz,

75kHz and 90kHz as shown in Fig. 7a, there are eleven waves at 150°C, with cut-ons occurring at about 10kHz, 12kHz, 22kHz, 68kHz, 78kHz, 102kHz and 109kHz as shown in Fig. 7b. Some of the waves exhibit modeshape change. This is observed as the point of curvature along the lines of the waves. Examples of such are the mode change of the flexural mode to axial at about 65kHz and of the axial mode to flexural at about 18kHz as shown in Fig. 7. The effect of temperature on the wavenumber magnitude can be analysed using the temperature dependent torsional wave dispersion relation shown in Fig. 8. Little difference in wavenumber is observed between -100°C and 90°C, whereas a significant difference of about 30% is observed between 90°C and 110°C, and beyond 110°C, the wavenumber increases at a steady rate. It is therefore evident that the panel's wavenumber will exhibit significant difference within and beyond the glass transition temperature range (90°C to 110°C).

[Figure 9 about here.]

The temperature dependent wave transmission loss of the layered panel is calculated using the approach presented in Section 3.2. The torsional wave transmission loss as a function of temperature is presented in Fig. 9. In a similar trend to the wavenumber results, the difference in the maximum dissipation ratio just before and after the glass transition range, is about 30% and maximum loss ratio is obtained within the range.

4.2. Temperature Dependent Wave Scattering Coefficients

The temperature dependent waves scattering coefficients of the waves interaction with damage along the layered panel is calculated as presented Section 3.3. Two forms of damage are studied, notch and crack. Notch is modelled by deleting elements along the line of the damage, as shown in Fig. 10. Crack is simply a notch of zero width. It is created by disconnecting the connecting nodes along the line of the crack to indicate surface breaking due to the crack [58].

As earlier stated, a system of two waveguides connected through a coupling joint(on which the damage is modelled) is considered. Each waveguide is a sandwich panel, comprising a honeycomb foam core and the upper and lower carbon fibre facesheets. The thickness of the core, h_c, is 10 mm while that of the lower facesheet, h_{c1}, is 1.0 mm and the upper facesheet, h_{c2}, is 2.0 mm. The

dimension of the panel is 1.0 mm $\times$ 5.0 mm. The panel is meshed using 1 mm (in each direction) elements. Hence, each waveguide has a total of 40 elements; 10 in the upper layer, 25 in the core and 5 in the lower layer. The coupling joint is modelled in the same manner as three segments of each waveguide in length, as shown in Fig. 6.

[Figure 10 about here.]

In the case of notch model, notch of 1 mm width and 2 mm depth is located at 1 mm from the left edge of the coupling joint. Similarly, a crack of 2 mm depth is modelled in the same location. In each case of the damage models, the WFE model of each waveguide is solved, then coupled with the solution of the FE model of the coupling element as explained in Section 3.3.

[Figure 11 about here.]

[Figure 12 about here.]

[Figure 13 about here.]

[Figure 14 about here.]

[Figure 15 about here.]

[Figure 16 about here.]

In both the crack and notch models, four classical propagating waves, which are flexural (in-plane and out-of-plane), torsional and axial waves, exist in the frequency range within 0.2kHz and 120kHz. Results of the reflection coefficients magnitude of these waves for the crack model are shown in Figs. 11, 12 and 13. Scattering coefficient trends of the axial and torsional waves show more sensitivity to change in temperature at higher frequencies in the range above 60kHz, while that of the flexural wave shows significant difference only in the range 25kHz to 85kHz but insignificant to temperature change outside this frequency range. The effect of temperature on the reflection coefficient below, within and after the glass transition temperature varies significantly. Below the glass transition temperature, there exist slight increase in the reflection coefficients of all

the wave types with a maximum difference of about 10% per 50°C change in temperature. Above the glass transition temperature, a considerable difference is observed with respect to temperature change with an observed difference of about 28% per 50°C change in temperature. Results for the reflection coefficients magnitude as a function of temperature for the notch model are presented in Figs. 14, 15 and 16. Compared to the notch model results, similar trend is observed in the crack model for the wave interaction coefficients relationship with temperature change, especially with regards to the glass transition range. Generally, the significance of the glass transition temperature range on the scattering properties along the panel is quite similar to that obtained for the panel's thermomechanical characteristics and wave propagation constants

5. Concluding remarks

The temperature dependent mechanical characteristics of a quasi-isotropic sandwich panel are presented in this article. The panel is made of two materials, carbon epoxy facesheet, impregnated in the resin and draped over the mould, and a quasi-isotropic honeycomb core. The thermomechanical characteristics of each of these materials are separately measured experimentally and it is observed that there is a large divergence of the material loss factor, elastic and shear moduli especially within and above the glass transition temperature of the resin. The thermomechanical characteristics are then used to determine the temperature dependent wave propagation properties of the panel using a wave finite element approach. An idealised system of two waveguides connected through a coupling element is considered. Two forms of damage; crack and notch are modelled along the coupling element. The wave finite element modelling of each waveguide segment is then coupled with the full finite element model of the coupling element (joint), on which damage is modelled, in order to calculate the temperature dependent scattering coefficients of the waves interaction with the damage. As in the case of the experimental results for the moduli and the material loss factor, the numerically predicted wave propagation properties and the wave scattering coefficients exhibit significant difference in their results before the glass transition temperature compared to that after the glass transition temperature. It can be concluded that temperature, especially at glass transition range, is a significant factor that should be taken into consideration in the design process of aerospace material in order to improve its wave response performance.

References

[1] S. S. Kessler, S. M. Spearing, C. Soutis, Damage detection in composite materials using lamb wave methods, Smart Materials and Structures 11 (2002) 269–78.

[2] C. Y. Lee, B. S. Thompson, M. V. Gandhi, Temperature-dependent dynamic mechanical properties of polymeric laminated beams, J. Eng. Mater. Technol 110 (1988) 174–9.

[3] A. J. Barker, H. Vangerko, Temperature dependent elastic constants of cfrp composites, Composites 14 (1983) 52–6.

[4] A. J. Barker, H. Vangerko, Temperature dependent dynamic shear properties of cfrp composites, Composites 14 (1983) 141–4.

[5] A. K. Noor, U. S. Burton, Computational models for high temperature multilayered composite plates and shells, Appl Mech Rev 45 (1992) 419–46.

[6] Y. I. Dimitrienko, Thermomechanical behaviour of composite materials and structures under high temperature: 1. materials, composites, Part A. Applied Science and Manufacturing 28 (1997) 463–71.

[7] Y. I. Dimitrienko, Thermomechanical behaviour of composite materials and structures under high temperature: 2. structures, composites, Part A. Applied Science and Manufacturing 28 (1997) 453–61.

[8] G. M. McNally, M. P. McCourt, P. L. Spedding, The effect of rapid high temperature excursions on the moisture absorption and dynamic mechanical properties of carbon fibre epoxy composite materials, development in chemical engineering and mineral processing, Asia-Pacific Journal of Chemical Engineering 12 (2004) 169–78.

[9] O. Putkis, R. P. Dalton, A. J. Croxford, The influence of temperature variations on ultrasonic guided waves in anisotropic cfrp plates, Ultrasonic 60 (2015) 109–16.

[10] G. Konstantinidis, P. D. Wilcox, B. W. Drinkwater, The long-term stability of guided wave structural health monitoring systems. review of progress in quantitative nondestructive evaluation, American Institute of Physics 25B (2006) 1702–9.

[11] G. Konstantinidis, B. W. Drinkwater, P. D. Wilcox, The temperature stability of guided wave structural health monitoring systems, Smart Materials and Structures 15 (2006) 967–76.

[12] T. Clarke, P. Cawley, P. D. Wilcox, A. J. Croxford, Evaluation of the damage detection capability of a sparse-array guided-wave shm system applied to a complex structure under varying thermal conditions, IEEE Transactions on Ultrasonics Ferroelectrics and Frequency Control 56 (2009) 2666–78.

[13] T. Clarke, P. D. Wilcox, P. Cawley, Guided wave health monitoring of complex structures by sparse array systems: influence of temperature changes on performance, Journal of Sound and Vibration 329 (2010) 2306–22.

[14] E. Blaise, F. K. Chang, Built-in diagnostics for debonding in sandwich structures under extreme temperatures, in Proceedings of the Third International Workshop on Structural Health Monitoring, Stanford University (2001) 154–63.

[15] B. C. Lee, G. Manson, W. J. Staszewski, Environmental effects on lamb wave responses from piezoceramic sensors, Material Science Forum 440–441 (2003) 195–202.

[16] M. J. Schulz, M. J. Sundaresan, J. Mcmichael, D. Clayton, R. Sadler, B. Nagel, Piezoelectric materials at elevated temperature, Journal of Intelligent Material Systems and Structures 14 (2003) 693–705.

[17] F. L. di Scalea, S. Salamone, Temperature effects in ultrasonic lamb wave structural health monitoring systems, Journal of Acoustical Society of America 124 (2008) 161–74.

[18] A. Marzani, S. Salamone, Numerical prediction and experimental verification of temperature effect on plate waves generated and received by piezoceramic sensors, Mechanical Systems and Signal Processing 30 (2012) 204–17.

[19] E. J. Cross, K. Worden, Approaches to nonlinear cointegration with a view towards applications in shm, Journal of Physics: Conference Series 305 (2011) 12069–78.

[20] E. J. Cross, K. Worden, Q. Chen, Cointegration: a novel approach for the removal of environmental trends in structural health monitoring data, Proceedings of the Royal Society of London 467 (2011) 2712–32.

[21] K. Worden, E. J. Cross, A. Kyprianou, Cointegration and nonstationarity in the context of multiresolution analysis, Journal of Physics: Conference Series 305 (2011) 12004–15.

[22] P. B. Dao, W. J. Staszewski, Cointegration approach for temperature effect compensation in lamb-wave-based damage detection, Smart Materials and Structures 22 (2013).

[23] R. S. Langley, P. J. Shorter, The wave transmission coefficients and coupling loss factors of point connected structures, Journal of the Acoustical Society of America 113 (2003) 1947–64.

[24] R. S. Langley, K. H. Heron, Elastic wave transmission through plate/beam junctions, Journal of Sound and Vibration 143 (1990) 241–53.

[25] I. Bosman, T. Nightingale, modelling vibrational energy transmission at bolted junctions between a plate and a stiffening rib, Journal of the Acoustical Society of America 109 (2001) 999–1010.

[26] S. A. F. M. Ishak, J. M. Horner, S. J. Walsh, modelling and experimentation of vibration transmission through an angled joint, 42nd International Conference and Exposition on Noise Control Engineering, Innsbruck, Austria (2013).

[27] S. K. Lee, B. R. Mace, B. M. J., Wave propagation, reflection and transmission in curved beams, Journal of Sound and Vibration 306 (2007) 636âĂŞ–656.

[28] M. Rucka, W. Witkowski, J. Chroscielewski, K. Wilde, Damage detection of a t-shaped panel by wave propagation analysis in the plane stress, Archives of Civil Engineering 58 (2012) 3–24.

[29] M. Rucka, Experimental and numerical study on damage detection in an l-joint using guided wave propagation, Journal of Sound and Vibration 329 (2010) 1760–79.

[30] J. M. Renno, B. R. Mace, Calculation of reflection and transmission coefficients of joints using a hybrid element/wave and finite element approach, Journal of Sound and Vibration 332 (2013) 2149–64.

[31] S. P. Shone, B. R. Mace, W. T. P., Estimation of reflection and transmission coefficients using the spectral element method: application to crack modelling in beams, in: International Conference on Noise and Vibration Engineering, Leuven 2004, ISMA, 2004, pp. 187âĂŞ–200.

[32] C. H. Wang, L. R. F. Rose, Wave reflection and transmission in beams containing delamination and inhomogeneity, Journal of Sound and Vibration 264 (2003) 851âĂŞ–872.

[33] S. P. Shone, B. R. Mace, T. P. Waters, Reflection and transmission coefficients using the spectral element method: Application to crack modelling in beams., Proceedings of Institute of acoustics Spring Conference, Institute of Sound and Vibration Research, Southampton, UK (2004).

[34] X. G. Zhao, J. L. Rose, Boundary element modelling for defect characterization potential in a wave guide, International Journal of Solids and Structures 40 (2003) 2645–58.

[35] M. Veidt, C. T. Ng, Influence of stacking sequence on scattering characteristics of the fundamental antisymmetric lamb wave at through holes in composite laminates, The Journal of the Acoustical Society of America 129 (2011) 1280–7.

[36] M. Castaings, E. Le Clezio, B. Hosten, Modal decomposition method for modelling the interaction of lamb waves with cracks, The Journal of the Acoustical Society of America 112 (2002) 2567–82.

[37] C. T. Ng, M. Veidt, H. F. Lam, Guided wave damage characterisation in beams utilising probabilistic optimisation, Engineering Structures 31 (2009) 2842–50.

[38] W. J. Zhou, M. N. Ichchou, Wave scattering by local defect in structural waveguide through wave finite element method, Structural Health Monitoring 10 (2011) 335–49.

[39] S. P. Shone, B. R. Mace, T. P. Waters, A combined finite and spectral element approach to wave scattering in a cracked beam: modelling and validation, Key Engineering Materials (2005) 541–8.

[40] G. Liu, A combined finite element/strip element method for analyzing elastic wave scattering by cracks and inclusions in laminates, Computational Mechanics 28 (2002) 76–82.

[41] J. M. Renno, B. R. Mace, Vibration modelling of structural networks using a hybrid finite element/wave and finite element approach, Wave Motion 51 (2014) 566–80.

[42] E. Manconi, B. R. Mace, Modelling wave propagation in two-dimensional structures using finite element analysis, ISVR Technical Memorandum 318 (2008) 884–902.

[43] D. Chronopoulos, B. Troclet, M. Ichchou, J. P. Laine, A unified approach for the broadband vibroacoustic response of composite shells, Composites Part B: Engineering 43 (2012) 1837–46.

[44] D. Chronopoulos, B. Troclet, O. Bareille, M. Ichchou, Modeling the response of composite panels by a dynamic stiffness approach, Composite Structures 96 (2013) 111–20.

[45] R. K. Apalowo, D. Chronopoulos, V. Thierry, Thermal effect on wave interaction in composite structures, 19th International Conference on Aerospace, Mechanical, Automotive and Materials Engineering, London, United Kingdom (2017).

[46] R. K. Apalowo, D. Chronopoulos, V. Thierry, Wave interaction with defects in pressurized composite structures, 19th International Conference on Aerospace, Mechanical, Automotive and Materials Engineering, London, United Kingdom (2017).

[47] D. Chronopoulos, M. Collet, M. Ichchou, Damping enhancement of composite panels by inclusion of shunted piezoelectric patches: A wave-based modelling approach, Materials 8 (2015) 815–28.

[48] D. Chronopoulos, I. Antoniadis, M. Collet, M. Ichchou, Enhancement of wave damping within metamaterials having embedded negative stiffness inclusions, Wave Motion 58 (2015) 165–79.

[49] D. Chronopoulos, I. Antoniadis, T. Ampatzidis, Enhanced acoustic insulation properties of composite metamaterials having embedded negative stiffness inclusions, Extreme Mechanics Letters (2016).

[50] D. Chronopoulos, Design optimization of composite structures operating in acoustic environments, Journal of Sound and Vibration 355 (2015) 322–44.

[51] D. Chronopoulos, Wave steering effects in anisotropic composite structures: Direct calculation of the energy skew angle through a finite element scheme, Ultrasonics 73 (2017) 43–8.

[52] E. Manconi, B. R. Mace, Modelling wave propagation in two-dimensional structures using a wave/finite element technique, ISVR Technical Memorandum (2007).

[53] B. R. Mace, D. Duhamel, M. J. Brennan, L. Hinke, Finite element prediction of wave motion in structural waveguides, The Journal of the Acoustical Society of America 117 (2005) 2835–43.

[54] W. X. Zhong, F. W. Williams, A. Y. T. Leung, Sympletic analysis for periodical electro-magnetic waveguides, Journal of Sound and Vibration 267 (2003) 227–44.

[55] F. Bloch, Über die quantenmechanik der elektronen in kristallgittern, Zeitschrift für physik 52 (1929) 555–600.

[56] J. M. Mencik, M. N. Ichchou, Multi-mode propagation and diffusion in structures through finite elements, European Journal of Mechanics-A/Solids 24 (2005) 877–98.

[57] ANSYS 14.0 User's Help, 2014.

[58] M. J. S. Lowe, C. P., J. Y. Kao, O. Diligent, The low frequency reflection characteristics of the fundamental antisymmetric lamb wave a0 from a rectangular notch in a plate, The Journal of the Acoustical Society of America 112 (2002) 2612–22.

List of Figures

Figure 1: Configuration of a segment of the facesheet traction test in the TMA device

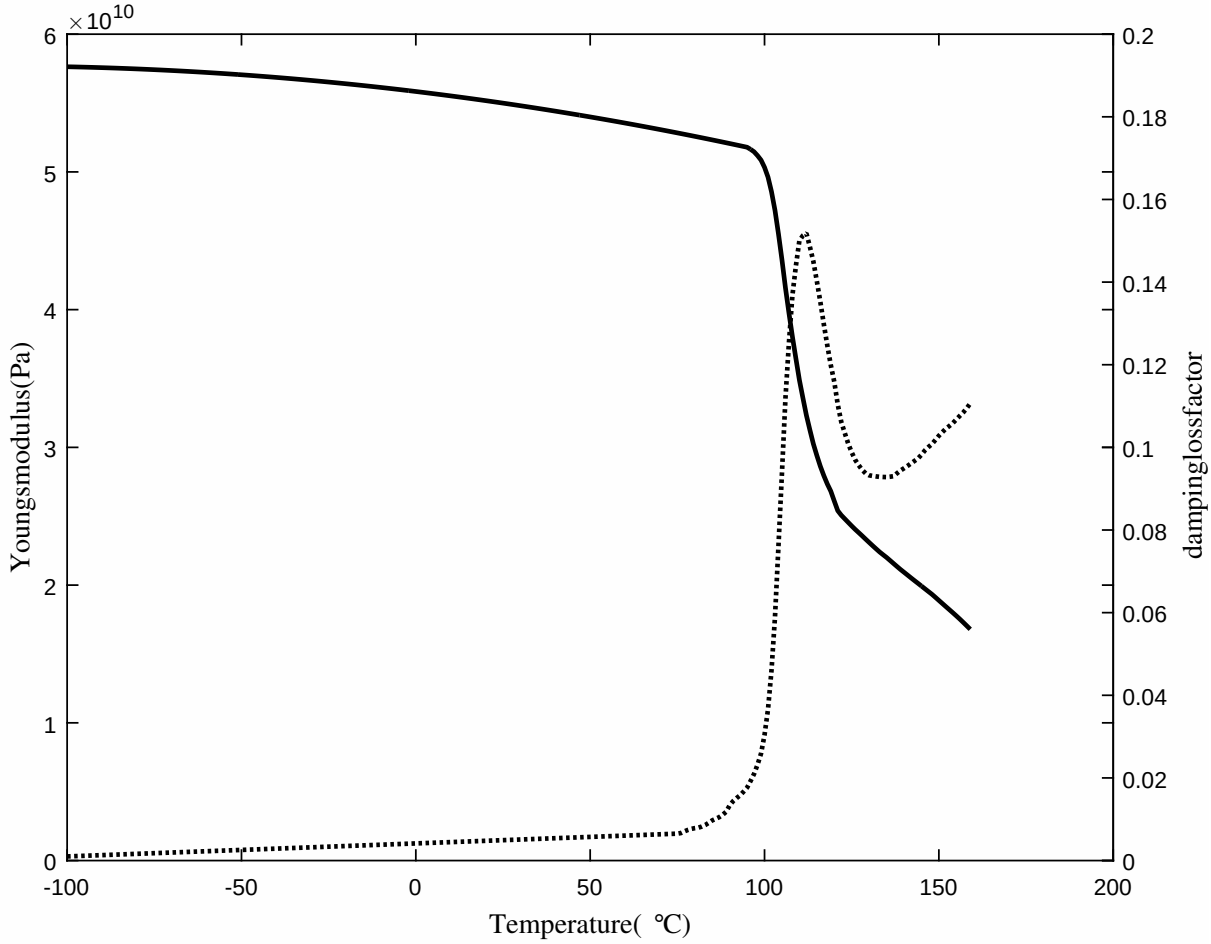

Figure 2: Experimentally measured temperature dependent elastic modulus (-) and material loss factor (⋯) for the facesheet material

Figure 3: Configuration of a segment of the core shear deformation in the TMA device

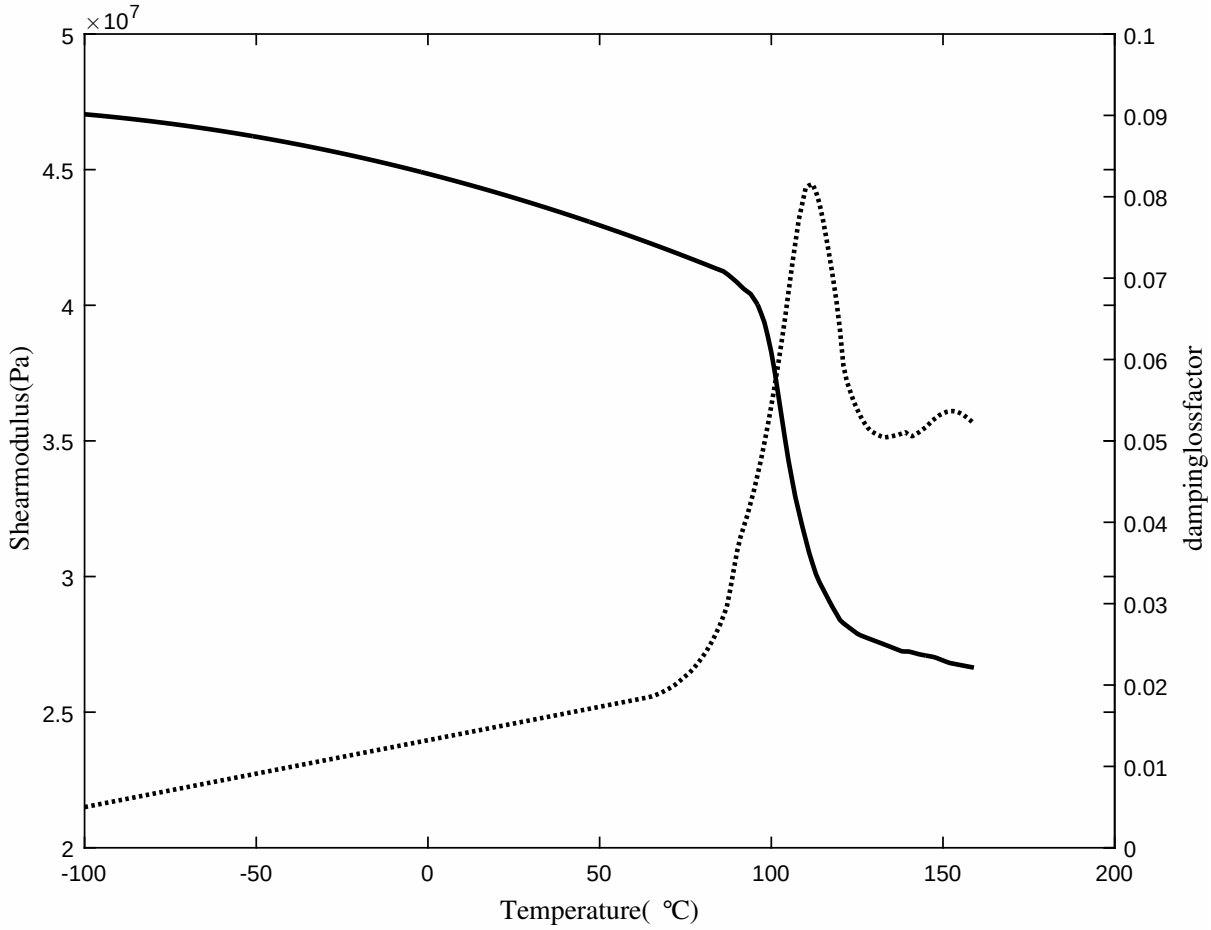

Figure 4: Experimentally measured temperature dependent shear modulus (-) and material loss factor (· · ·) for the honeycomb core material

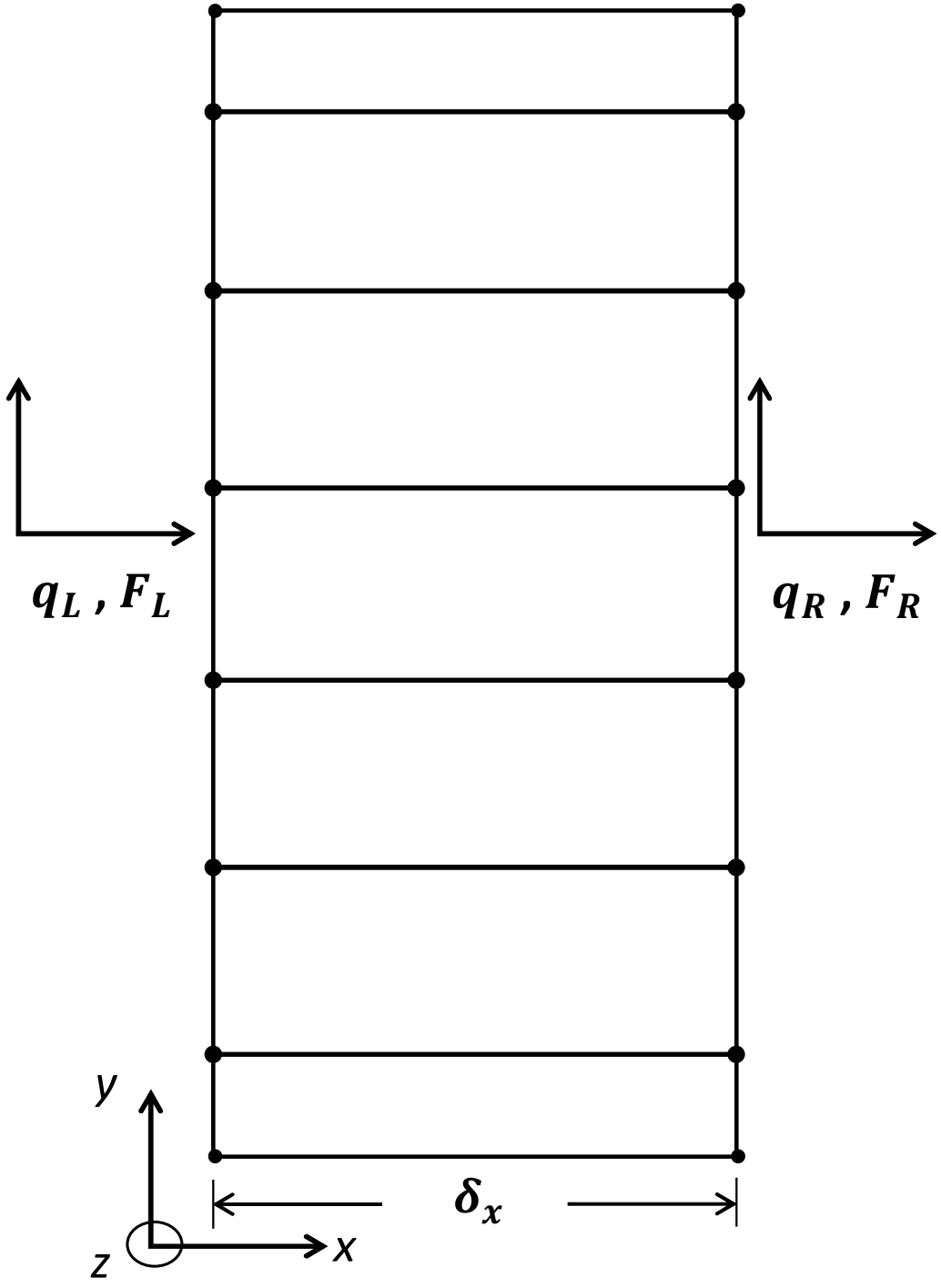

Figure 5: Finite element mesh of the section of the waveguide's segment

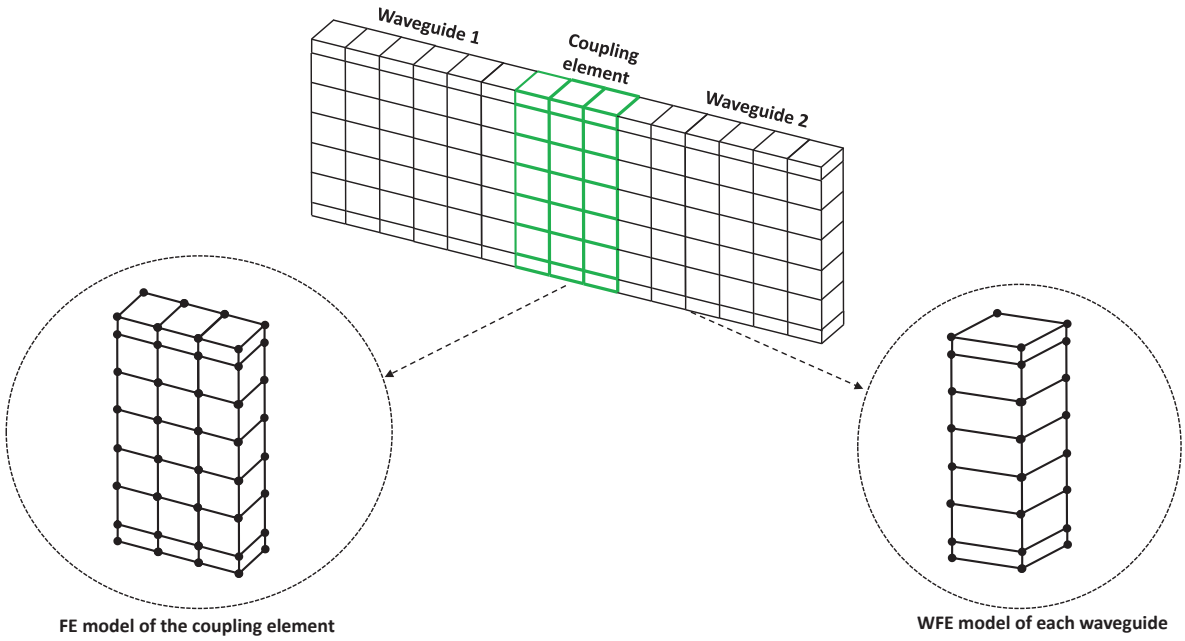

Figure 6: Caption of a system of two coplanar waveguides connected through a coupling joint/element, the WFE model of each waveguide and standard FE model of the joint

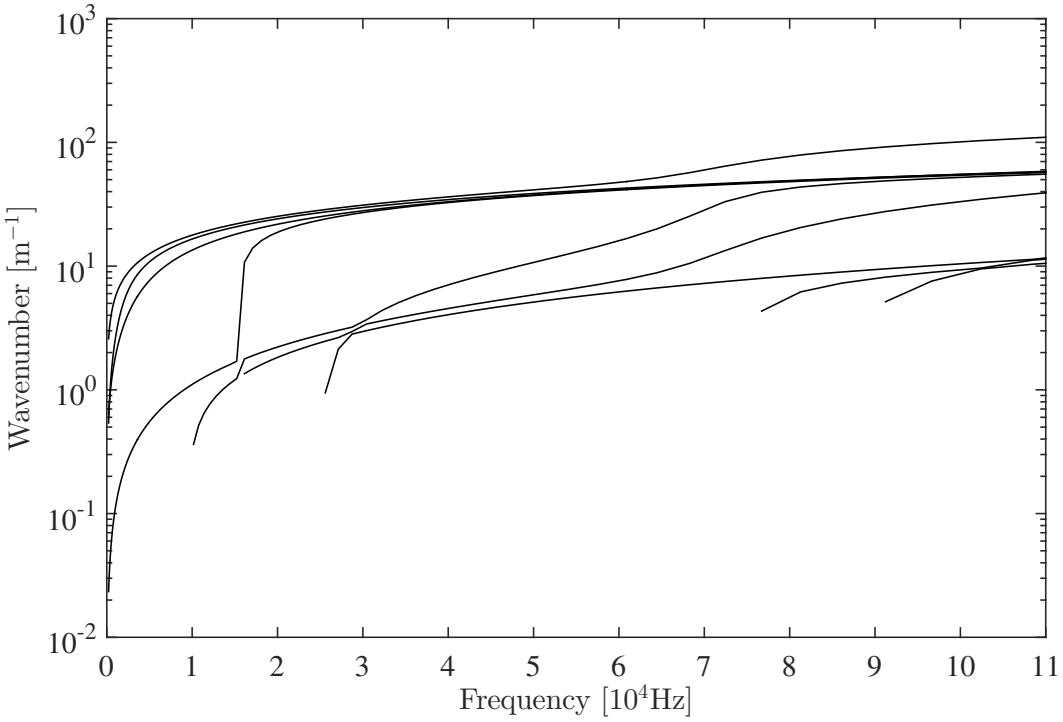

(a) 25°C

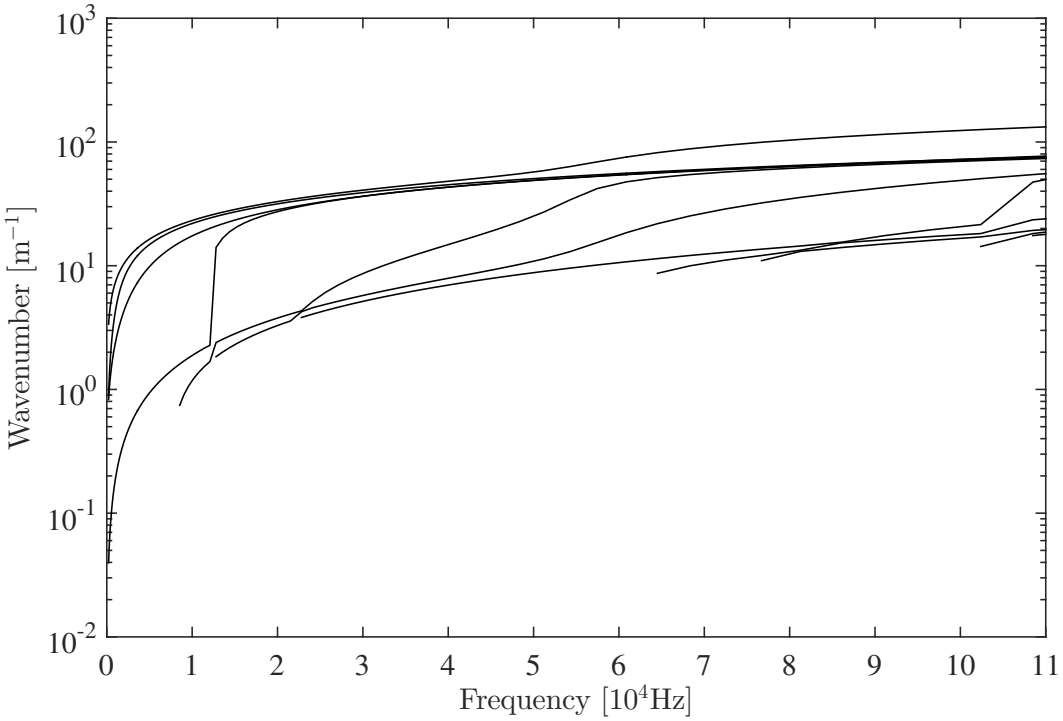

(b) 150°C

Figure 7: Dispersion relations for waves in the composite panel at 25°C and 150°C

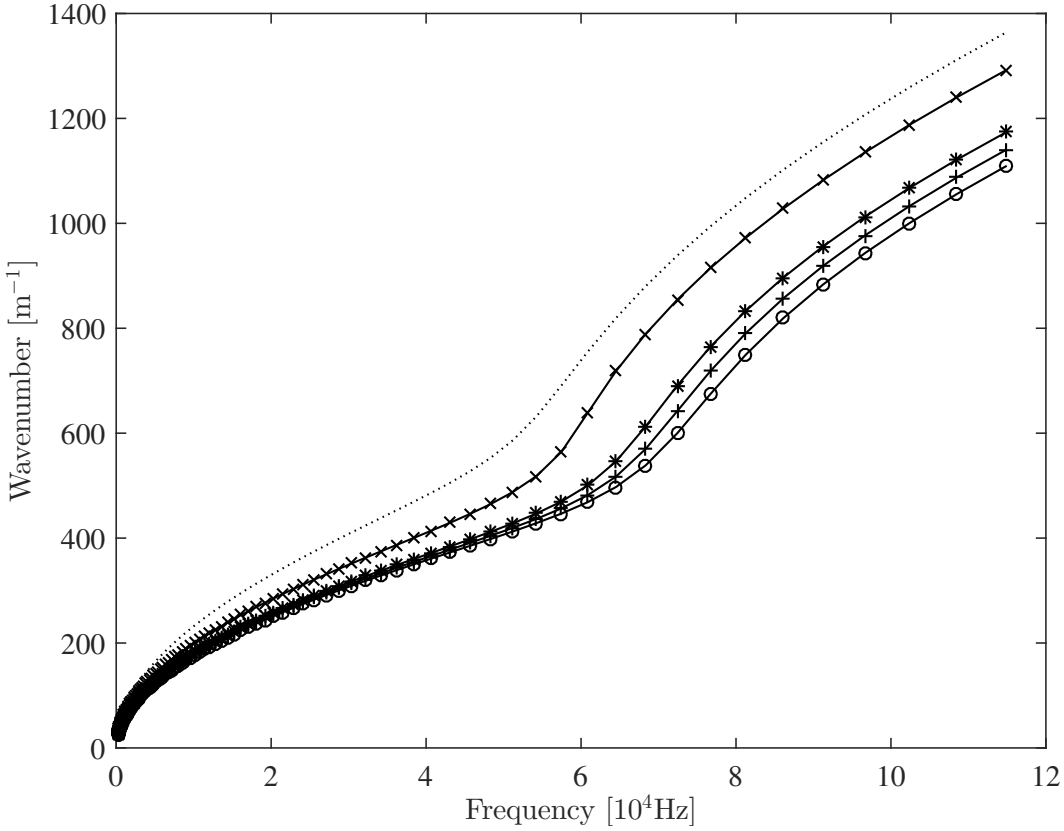

Figure 8: Dispersion relations for torsional waves in the composite panel at -100°C (o), 25°C (+), 90°C (*), 110°C (x) and 150°C ($\cdots$)

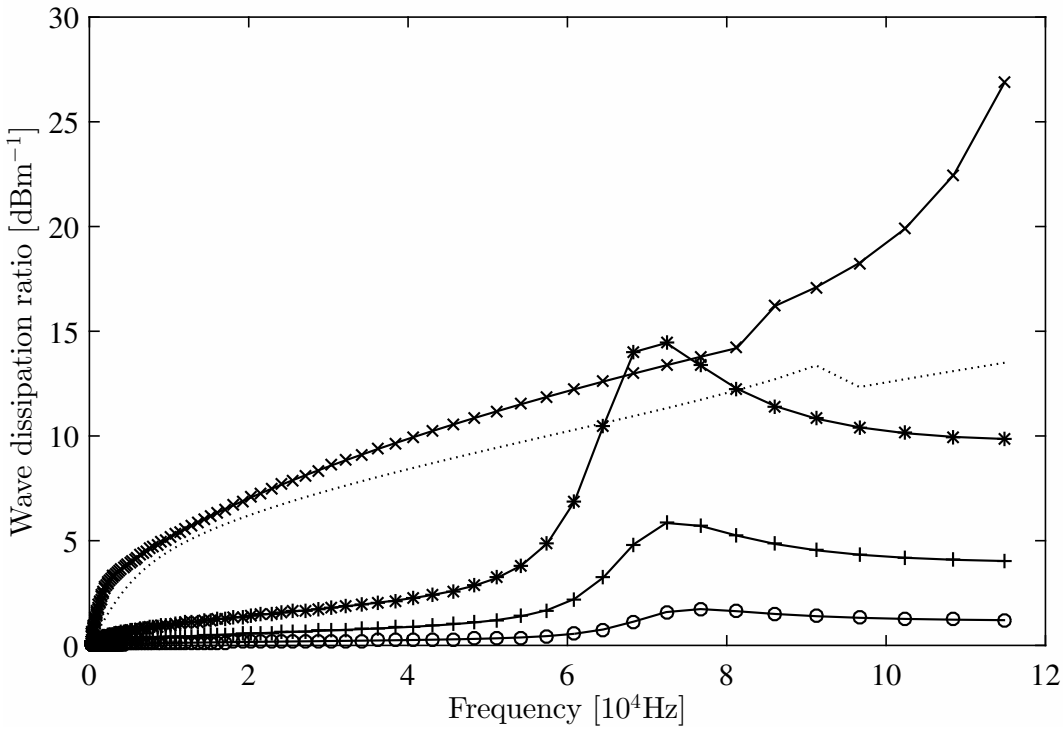

Figure 9: Predicted temperature dependent dissipation ratio of the layered panel for flexural wave at -100°C (o), 25°C (+), 90°C (*), 110°C (x) and 150°C ($\cdots$)

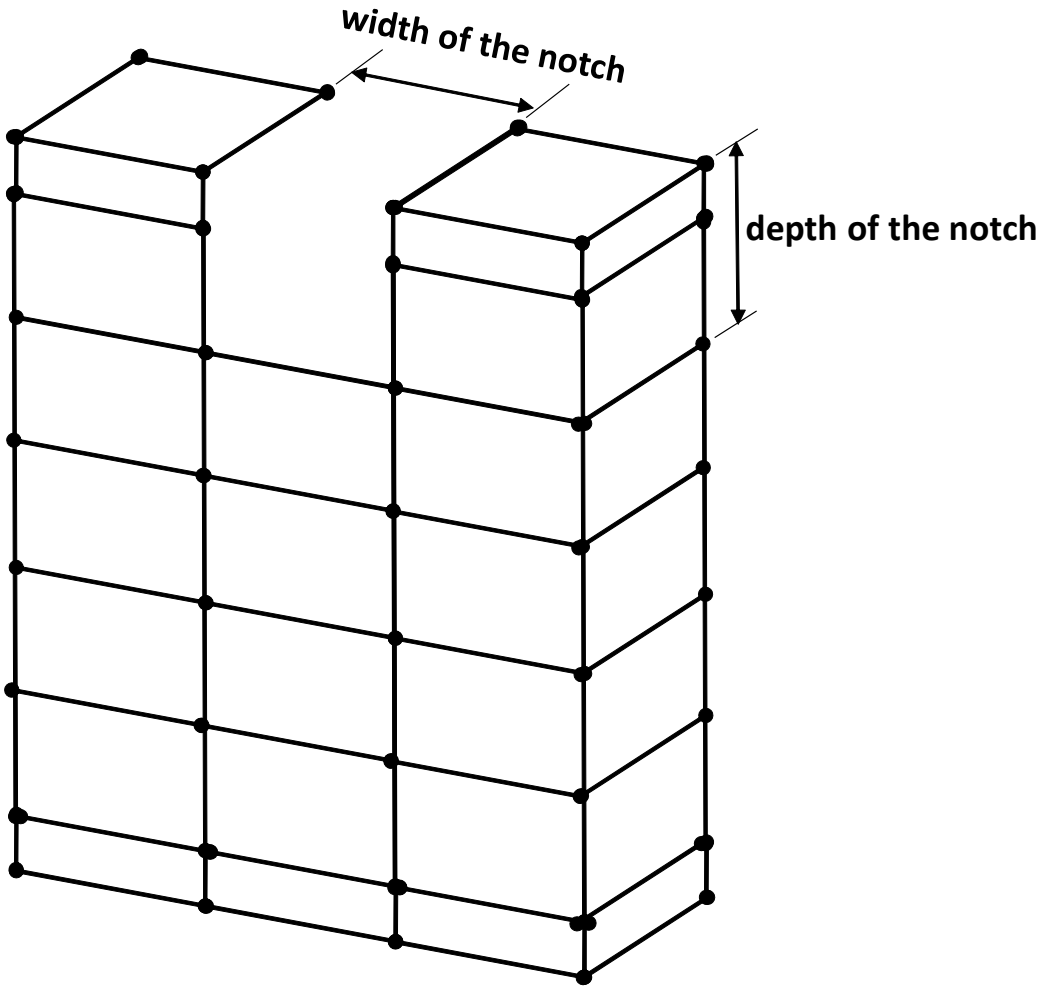

Figure 10: FE mesh of the coupling element showing region of the notch

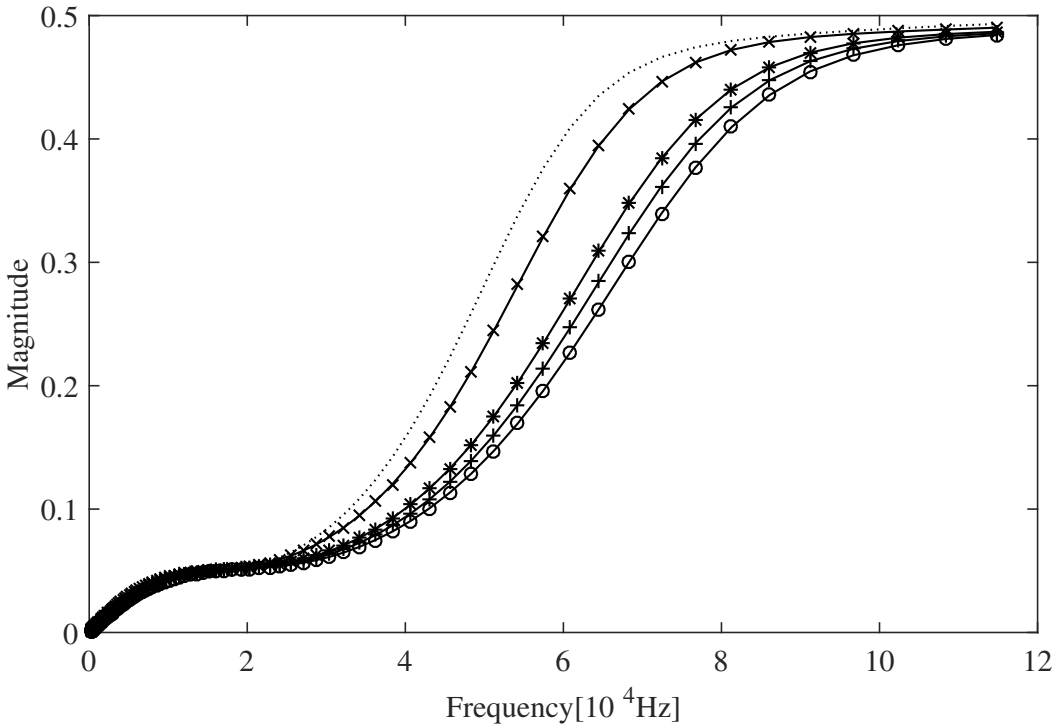

Figure 11: The temperature dependent reflection coefficient magnitude of the flexural wave from cracked joint of the panel at -100°C (o), 25°C (+), 90°C (*), 110°C (x) and 150°C ($\cdots$)

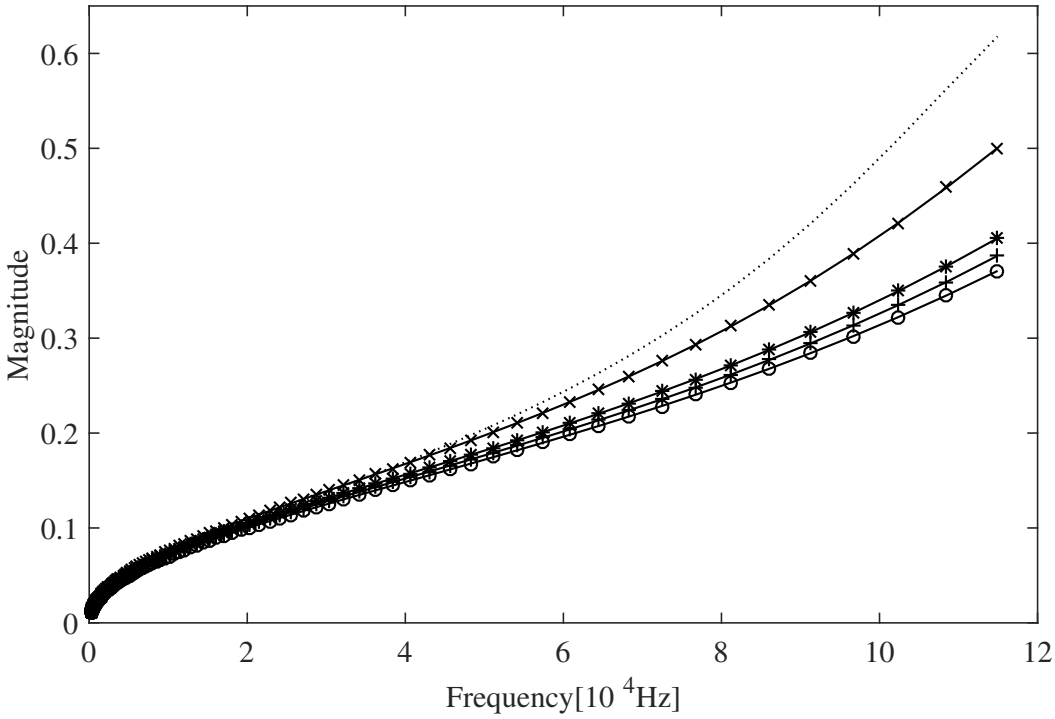

Figure 12: The temperature dependent reflection coefficient magnitude of the torsional wave from cracked joint of the panel at -100°C (o), 25°C (+), 90°C (*), 110°C (x) and 150°C ($\cdots$)

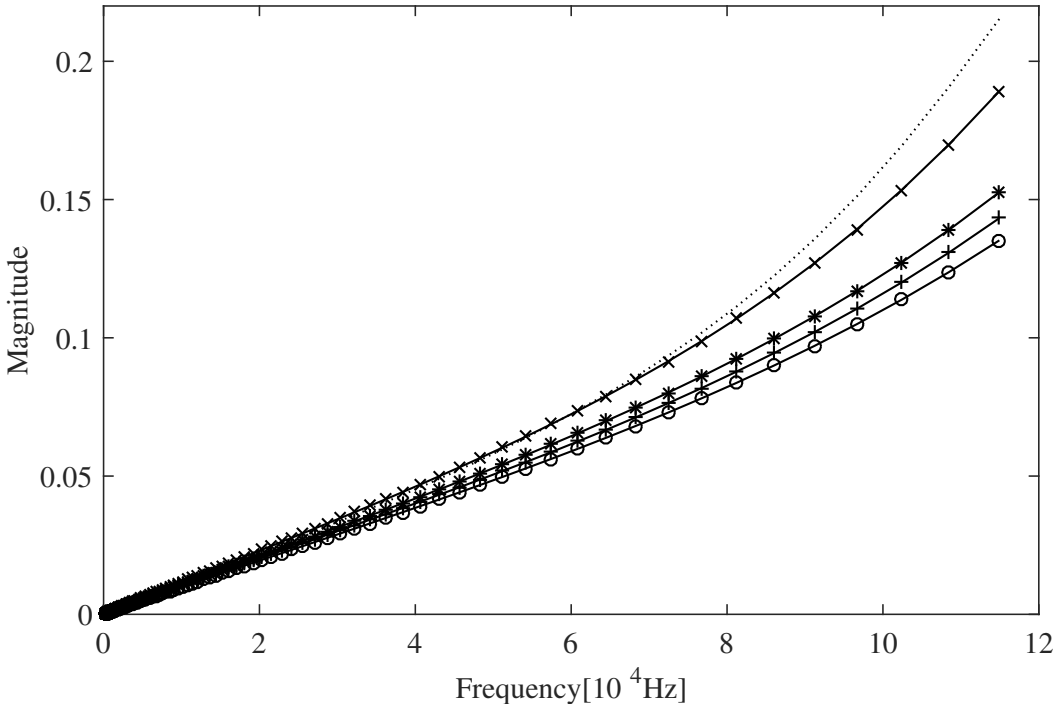

Figure 13: The temperature dependent reflection coefficient magnitude of the axial wave from cracked joint of the panel at -100°C (o), 25°C (+), 90°C (*), 110°C (x) and 150°C ($\cdots$)

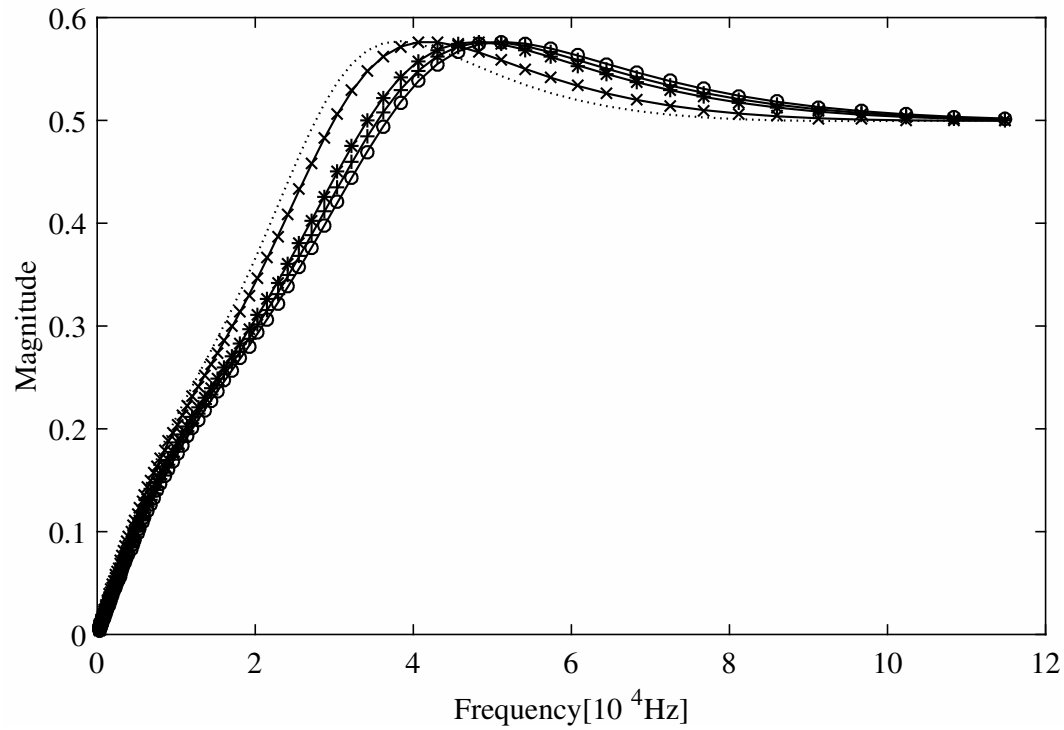

Figure 14: The temperature dependent reflection coefficient magnitude of the flexural wave from notched joint of the panel at -100°C (o), 25°C (+), 90°C (*), 110°C (x) and 150°C ($\cdots$)

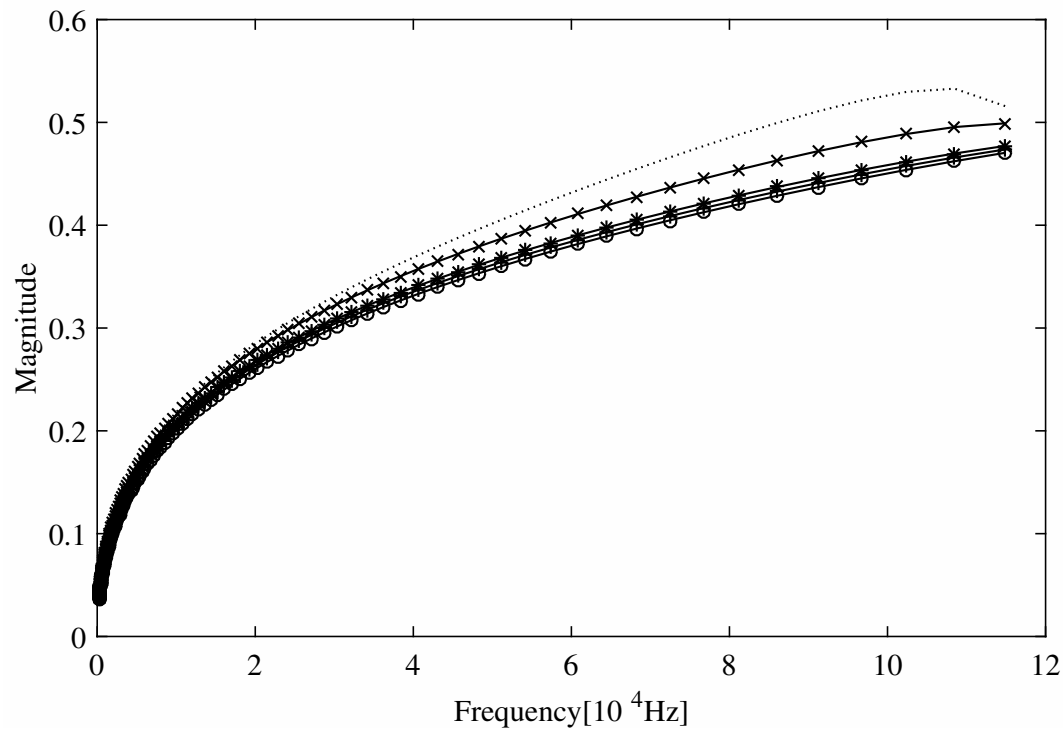

Figure 15: The temperature dependent reflection coefficient magnitude of the torsional wave from notched joint of the panel at -100°C (o), 25°C (+), 90°C (*), 110°C (x) and 150°C ($\cdots$)

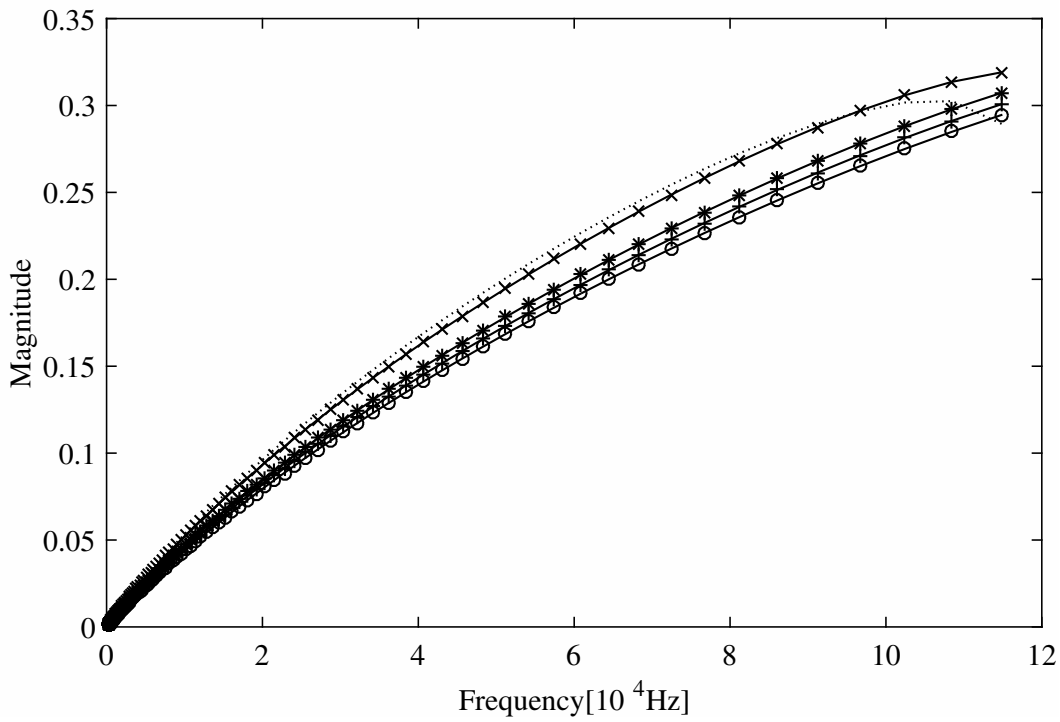

Figure 16: The temperature dependent reflection coefficient magnitude of the axial wave from notched joint of the panel at -100°C (o), 25°C (+), 90°C (*), 110°C (x) and 150°C ($\cdots$)

List of Tables

Table 1: Nominal mechanical properties of the composite panel's constituents at 20°C

Carbon Epoxy	Honeycomb foam
E = 54 GPa	E_x = 85 MPa
ρ = 1410 kg/m^3	E_y = 85 MPa
ν = 0.09	ρ = 48 kg/m^3
	ν_{xy} = 0.23
	G_{yz} = 44 MPa
	G_{xz} = 44 MPa